Isocyanide Ligation Enables Electrochemical Ammonia Formation in a Synthetic Cycle for N_2 Fixation

Jeremy E. Weber,[1,†] Noah D. McMillion,[2,†] Alexander S. Hegg,[1,†] Ashlee E. Wertz,[3] Mehrnaz Aliahmadi,[2] Brandon Q. Mercado,[1] Robert H. Crabtree,[1] Hannah S. Shafaat,[3,4,] Alexander J. M. Miller,[2,*] and Patrick L. Holland[1,*]*

[1] Department of Chemistry, Yale University, New Haven, CT

[2] Department of Chemistry, University of North Carolina, Chapel Hill, NC

[3] Department of Chemistry and Biochemistry, The Ohio State University, Columbus, OH

[4] Department of Chemistry and Biochemistry, University of California, Los Angeles, CA

[†]Equal contribution

Abstract

Transition-metal-mediated splitting of N_2 to form metal nitride complexes could constitute a key step in electrocatalytic nitrogen fixation, if these nitrides could be electrochemically reduced to ammonia under mild conditions. The envisioned nitrogen fixation cycle involves several steps: N_2 binding to form a binuclear end-on bridging complex with appropriate electronic structure to cleave the N_2 bridge followed by proton/electron transfer to release ammonia and bind another molecule of N_2. The nitride reduction and N_2 splitting steps in this cycle have differing electronic demands that a catalyst must satisfy. Rhenium systems have had limited success in meeting these demands, and studying them offers an opportunity to learn strategies for modulating reactivity. Here, we report a rhenium system in which the pincer supporting ligand is supplemented by an isocyanide ligand that can accept electron density, moderating the redox potentials and enabling the protonation/reduction of the nitride to ammonia under mild electrochemical conditions. The incorporation of isocyanide raises the N–H bond dissociation free energy of the first N–H bond by 10 kcal/mol, breaking the usual compensation between pK_a and redox potential; this is attributed

to the spatial separation of the protonation site (nitride) and the reduction site (isocyanide). Ammonia evolution is accompanied by formation of a terminal N_2 complex, which can be oxidized to yield bridging N_2 complexes including a rare mixed-valent complex. These rhenium species define the steps in a synthetic cycle that converts N_2 to NH_3 through an electrochemical N_2 splitting pathway, and show the utility of a second supporting ligand for enhancing nitride reactivity.

Introduction

The Haber–Bosch process (HBP, eq 1) converts dinitrogen (N_2) to ammonia (NH_3) on the industrial scale.[1-2] NH_3 is the key precursor to all N-containing fertilizers, commodity chemicals, and pharmaceuticals, which contributes to the huge scale of the HBP.[1, 3-4] Although the HBP constitutes a critical transformation, it is currently linked to fossil fuels since the H_2 used for integrated HBP systems comes from methane by way of the water-gas shift reaction.[2] One alternative to the HBP is electrocatalytic nitrogen reduction (ENR), which can break the link between N-containing products and fossil fuels by eliminating the need for H_2 as a reactant while also alleviating the need for high reaction temperatures and pressures (eq 2).[5-9] Furthermore, low-pressure ENR could be conducted on a small scale with solar energy, air, and water, providing the opportunity for local NH_3 synthesis that reduces the economic and environmental costs of the large fertilizer distribution network.[6,9] However, ENR requires an efficient catalyst with fast rates, and current electrocatalysts have not yet reached rates that make them scalable.[10-17]

$$\text{HBP: } N_2 + 3\ H_2 \longrightarrow 2\ NH_3 \quad (1)$$

$$\text{ENR: } N_2 + 8\ H^+ + 6\ e^- \longrightarrow 2\ NH_4^+ \quad (2)$$

Efforts toward the development of molecular catalysts for N_2 reduction to NH_3 through eq 2 have utilized chemical reductants and organic acids to deliver the e^- and H^+ equivalents.[18-19] The

first example of a catalytic molecular system was achieved by Schrock using a tripodal Mo complex.[20-21] Nishibayashi greatly improved the turnover number (TON) through the use of pincer-supported Mo complexes, which are still the preeminent molecular catalysts using chemical reductants displaying turnover numbers (TONs) of over 60,000.[22-23] Recently, these have also been found to be electrocatalysts at –1.89 V with about 12 turnovers.[24]

Along with catalyst development, important work has addressed the choices of acids and reducing agents. The Mo-based catalysts above typically used strong metallocene reductants and protic acids to provide a strong driving force.[18] Nishibayashi demonstrated catalysis using SmI_2/alcohol mixtures,[25-26] which are proposed to deliver the electrons and protons through a concerted addition pathway (proton-coupled electron transfer, PCET).[27-29] Peters achieved electrochemical PCET to N_2 complexes of Mo and W, which can be facilitated with cobaltocene-based PCET mediators.[24, 30] In a complementary approach, photosensitizers have been used to generate high-energy H• equivalents: Nishibayashi used an Ir photoredox catalyst in combination with acridine to reduce a pincer-supported Mo nitride to ammonia,[31] and Peters used a Hantzsch ester as photosensitizer.[32]

The pincer-supported Mo catalysts that dominate the field are most often proposed to produce NH_3 through an N_2 splitting mechanism (Figure 1).[13, 18-19, 33-35] (For brevity, we do not discuss catalysts that use other mechanisms, and refer the reader to recent reviews.[18-19]) The first part of the cycle is N_2 splitting. This begins with binding of N_2 to one metal center to form a terminal N_2 complex (MNN), followed by formation of a bimetallic complex in which N_2 has an end-on/end-on bridging mode (MNNM).[36-37] The relative energies of terminal versus bridging bimetallic N_2 complexes may be understood using qualitative MO diagrams of the π-system of the MNNM unit (middle of Figure 1).[38-40] For tetragonal complexes, splitting occurs when the π-

orbital manifold has 10 electrons (π^{10}), activating the N–N bond and producing a nitride that is stabilized by maximal π-bonding.[39, 41-42] These 10 π electrons come from the π-bonding orbitals of N_2 ($4e^-$) and the metal valence orbitals with the correct symmetry ($3e^-$ each, which requires d^5 for a four-fold symmetric metal fragment because two electrons lie in *d* orbitals that do not engage in π-bonding with N_2).[39-40] In addition to this electronic requirement, each metal fragment ideally has an open coordination site *trans* to N_2, which can lower the energy input required for N_2 splitting and enhance the strength of the metal-nitride bond in the product.[13, 41, 43-45]

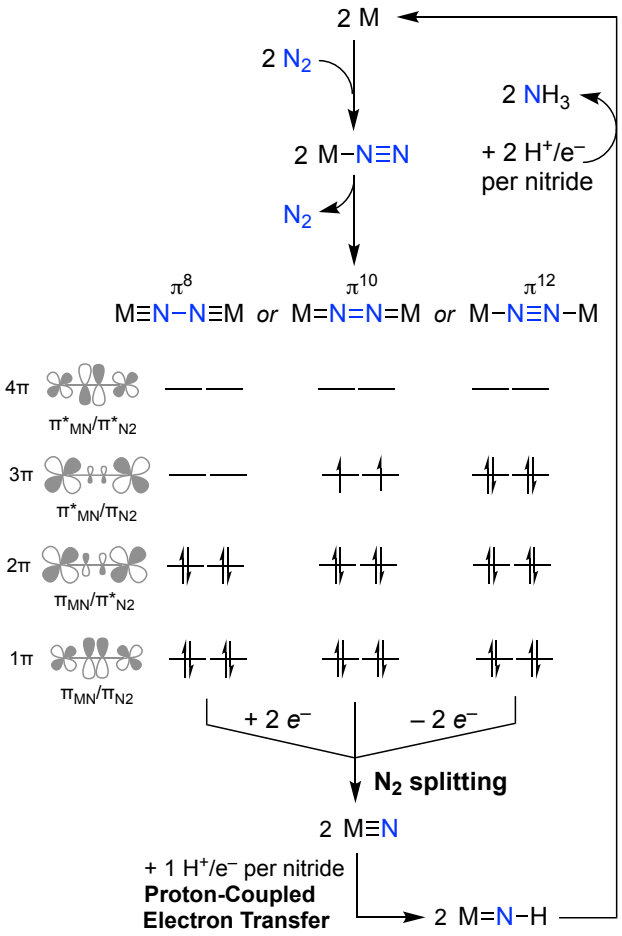

Figure 1. An N_2 splitting and ammonia production cycle, highlighting the two main steps, N_2 splitting and PCET nitride reduction. The figure also shows the configurations of the π-orbital manifold for tetragonal complexes; each must attain a π^{10} configuration to split N_2.

Sometimes, a bridging N_2 complex requires oxidation or reduction to reach a π^{10} configuration that enables N_2 splitting. As examples, consider two complexes that do *not* undergo N_2 splitting, $[(depe)_2Mo]_2(\mu\text{-}N_2)$ (depe = 1,2-bis(diethylphosphino)ethane) which is π^{12} and best depicted as Mo–N≡N–Mo,[46] and $[(PNP^{tBu})ReCl]_2(\mu\text{-}N_2)$ (PNP^{tBu} = $^tBu_2PCH_2CH_2NCH_2CH_2P^tBu_2$) which is π^8 and best depicted as Re≡N–N≡Re.[47] Oxidation of the π^{12} complex, or reduction of the π^8 complex, leads to the favored π^{10} configuration that is best depicted as M=N=N=M, and then N_2 splitting occurs.[39-40]

In principle, these guidelines should enable the use of a variety of transition metals for catalytic NH_3 production through an N_2 splitting mechanism. However, the field is still dominated by Mo and W catalysts.[18-19] Rhenium is an interesting case because a number of Re-based N_2 splitting systems are also known,[45, 47-50] but only two papers with Re catalysts have been reported.[51-52] Thus, it is a worthy test case for how to convert an N_2-splitting system into a catalyst.

Following N_2 splitting, traversing the remainder of the cycle depends on the second stage of the mechanism in Figure 1: PCET reduction of the nitride complex to furnish ammonia. A key challenge to favorable PCET is that the preceding N_2 splitting step is typically driven by the formation of a strong metal-nitride bond, making it energetically costly to reduce the M–N bond order to give the imido (M=NH) species. This corresponds to a low N–H bond dissociation free energy (BDFE, eq. 3).[13, 53-54] The low N–H BDFE can make it challenging to find H^+/e^- donors that are sufficiently active to drive PCET to the nitride.[55-57]

$$M{\equiv}N + H\bullet \xrightarrow{\Delta G = -\text{BDFE (N–H)}} M{=}NH \qquad (3)$$

This explains why successful Mo-based catalytic systems use H• donors with low BDFE values (*e.g.* SmI_2/ROH) or mixtures of reducing agents and acids with low "effective BDFE" (*e.g.* $KC_8/HBAr^F{}_4$; Ar^F = 3,5-$(CF_3)_2C_6H_3$).[18-19] An "effective BDFE" is the total thermodynamic driving

force from PCET (eq 4; C_G is a constant that depends on the solvent),[27, 55, 58-60] and a low effective BDFE comes from the use of a strong reductant and/or a strong acid. On the other hand, mild conditions for catalysis require the use of weaker reductants and/or weaker acids, corresponding to less overpotential for eventual ENR.

$$\text{BDFE (N–H)} = 1.37\ \text{p}K_a(\text{M=NH}) + 23.06\ E^0\ (\text{M}\equiv\text{N}) + C_G \quad (4)$$

Eq 4 is useful because it conceptually separates pK_a and $E°$ effects. Formation of a strong N–H bond may be facilitated with a more Brønsted basic nitride and/or a less reducing nitride. Viewed in this context, it is evident that an obstacle to mild catalysis is that reduction potentials of *N_2-derived* nitrides are often extremely negative (< –2.0 V vs. $Fc^{+/0}$).[45-46, 61-63] This contrasts with the non-N_2-derived nitride complexes with more positive potentials that lead to stronger N–H bonds[64-66] and readily form ammonia, like the Os^{IV}(N)(tpy)(bpy) system of Meyer[67] and the (PNP)Ru(N) system of Schneider.[68-69] Chirik has quantified the thermodynamics of PCET to a number of nitrides,[59] and driven PCET to nitride with photochemistry.[70-72]

A crucial need in this area is to develop guidelines that can be used to increase the N–H BDFE for nitrides derived from N_2 splitting.[38, 59] By providing a strong driving force, the catalytic systems that use an N_2 splitting mechanism have overcome this obstacle, but the field lacks principles that enable tuning of an unreactive nitride into one that can yield ammonia under mild conditions. Here, we present a rare example of a N_2-derived nitride that can generate NH_3 in high yields under mild conditions (room temperature, electrochemical reduction, weak acid). The reduction of the nitride to ammonium also yields an N_2 complex, which may be cleaved to complete a synthetic cycle.

The work described here builds upon the previously reported (^{Pyrr}PNP)Re(N)Cl (**1**), in which ^{Pyrr}PNP is a bis-phosphine pyrrolyl L_2X pincer (see Scheme 1 below), which can come from

N_2 splitting.[50] Nitride **1** was unreactive toward acids and reductants, and we surmised that the N–H BDFE in the desired intermediate (^{Pyrr}PNP)Re^{IV}(NH)Cl is too weak. Since reduction of nitride complex **1** occurred at potentials more cathodic than –3 V vs. $Fc^{+/0}$ in THF, we hypothesized that the low $Re^{V/IV}$ redox potential was the main contributor to the weak N–H BDFE. Here, we exchange the anionic chloride for a neutral isocyanide. This second supporting ligand can act as a π-acceptor and makes the Re^{V} nitride complex cationic and easier to reduce. We show that this redox tuning strategy gives a system that can both cleave N_2 *and* undergo PCET at the nitride product to form NH_3. With this next-generation nitride, ammonia formation followed by N_2 binding can be achieved electrochemically, followed by thermal N_2 splitting to complete a synthetic cycle for electrochemical ammonia production. Further, we isolate and characterize rhenium-N_2 intermediates that give mechanistic insight into the individual steps of the reaction.

Results

Reactivity of a Cationic Rhenium(V) Nitride Complex Bearing an Isocyanide Ligand. As noted above, chloride complex **1** can be generated from splitting of N_2, though for convenience we typically generated it from an alternative method described in the Supporting Information. We first substituted the chloride in **1** with xylyl isocyanide (CNXyl; Xyl = 2,6-dimethylphenyl), producing [(^{Pyrr}PNP)Re(N)(CNXyl)][PF_6] (**2**) which was crystallographically characterized (Figure 3A, Table 1) in 60% yield. Ison has described a rhenium(V) nitride isocyanide complex with a different PNP pincer, though its infrared spectrum was not reported.[73] Infrared (IR) spectra of **2** showed bands at 1089 (1073 with $Re^{15}N$) and 1077 (1050 with $Re^{15}N$) cm^{-1}, for which the shift with ^{15}N labeling at the nitride indicates Re–$N_{nitride}$ stretching character. Additionally, there was an isotope-insensitive band at 2141 cm^{-1} that is assigned as a C≡N_{Xyl} stretching mode. It lies

at a higher frequency than free CNXyl (2119 cm^{-1}), which suggests that there is little π-backbonding from the high-valent rhenium(V) center into the isocyanide.[74] This interpretation is consistent with the short C–N distance of 1.156(5) Å.

Cyclic voltammetry (CV) was used to compare the reduction potentials of the neutral complex **1** and cationic complex **2** in 0.2 M $[NBu_4][PF_6]$ in fluorobenzene (PhF). For **1**, no reductions were observed up to the PhF solvent window (ca. –3.2 V vs. $Fc^{+/0}$, Figure 2, black trace). Complex **2**, on the other hand, showed reduction waves at –1.79 and –2.35 V vs. $Fc^{+/0}$ that are assigned as $Re^{V/IV}$ and $Re^{IV/III}$ couples, respectively (see Supporting Information for details and CV in THF solvent). Overall, replacing an anionic Cl^- ligand with a neutral CNXyl ligand generates a cationic complex that is easier to reduce.

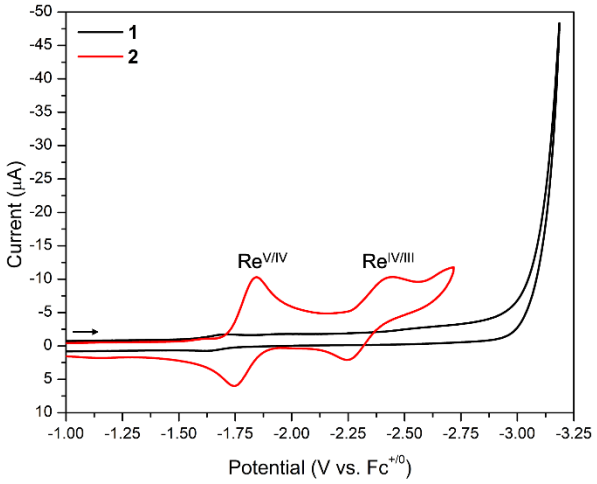

Figure 2. Cyclic voltammograms (100 mV/s) of **1** (black) and **2** (red) taken in PhF with 0.2 M $[NBu_4][PF_6]$. Glassy carbon working electrode, $Ag^{+/0}$ reference electrode, Pt wire counter electrode. The second reduction wave in **2** is quasi-reversible; see SI for details.

Scheme 1. Synthesis of compounds **1**-**3**.

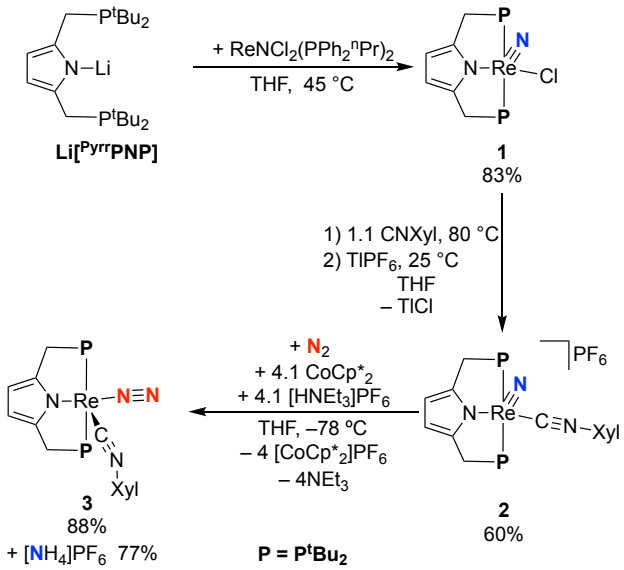

Next, we tried to form N–H bonds through addition of various reductant/acid combinations to **2** (Table S1). While SmI_2/ethylene glycol gave the best yields (up to 1.5 equiv NH_4^+/Re), we opted to concentrate on reagents that would transfer protons and electrons sequentially, for analogy to the envisioned electrochemical nitride reduction outlined above. The cleanest transformation came in the presence of $CoCp^*_2$, a reductant with reducing power similar to the reduction in the CV. Addition of $CoCp^*_2$ to **2** followed by addition $[HNEt_3][PF_6]$ dropwise in THF at –78 °C under an N_2 atmosphere led to a new product **3** in 88% yield as judged by ^{1}H NMR spectroscopy (Scheme 1).

NMR and X-ray diffraction studies identified **3** as the rhenium(I) complex (^{Pyrr}PNP)Re(N_2)(CNXyl) (Figure 3, Table 1). In this complex, a terminal N_2 ligand is coordinated in the plane of the pincer ligand, and it shows a N–N stretching band at 1996 cm^{-1} (1942 cm^{-1} for **3**–^{15}**N$_2$**) in its IR spectrum. The N–N bond length is 1.121(4) Å, which is close to that in free N_2.[37] The isocyanide shifts away from the rhenium-pincer plane (Figure 3), with the N_{Pyrr}–Re–$C_{isocyanide}$ angle changing from 150° in **2** to 114° in **3**; thus the isocyanide is in a basal position in **2**, but in

an axial position in **3**. Additionally, the C≡N_{Xyl} bond length lengthens to 1.214(4) Å, the C–N–Xyl angle bends to 142°, and the C≡N_{Xyl} stretching frequency lowers to 1807 cm^{-1}, demonstrating greater backbonding into the isocyanide in **3**. This backbonding explains why the N_2 is less activated than in other rhenium(I) complexes.[75]

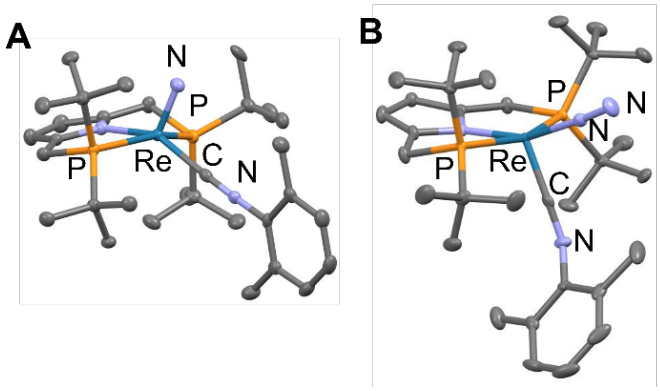

Figure 3. Solid-state structures of complexes **2** (A) and **3** (B) with thermal ellipsoids at 50% probability. Hydrogen atoms and PF_6^- are omitted for clarity.

Table 1. Key bonding metrics for **1**, **2**, and **3**. Frequencies in cm^{-1}, distances in Å, angles in deg.

	1	**2**	**3**
ν_{Re-N}	1091, 1071	1089, 1073	536
ν_{N-N}			1996
ν_{C-N}		2141	1807
Re–N (Nitride / N_2)	1.652(4)	1.648(3)	1.9563(3)
Re–C		2.034(4)	1.860(3)
Re–N (PNP)	2.049(4)	2.053(3)	2.056(2)
C–N (isocyanide)		1.156(5)	1.214(4)
N–Re–N	108.25(18)	112.62(14)	158.71(11)
C–Re–N (PNP)		149.73(14)	113.61(21)
N(Nitride / N_2)–Re–C		97.51(16)	87.67(13)
C–N–C (isocyanide)		171.4(4)	142.2(3)

In order to determine the fate of the nitrido ligand during the conversion of **2** to **3**, we repeated the reduction of **2** in the presence of $[HNEt_3][PF_6]$, but instead of isolating the rhenium product the mixture was treated with base and the volatile components were collected and acidified (see Supporting Information for details). Ion chromatography (IC) indicated a 77% yield of NH_4^+. Isotopically labeled **2–^{15}N** gave $^{15}NH_4$ (>99% isotopic purity, Figure S28), confirming that the ammonium originates from the nitride in **2**.

Electrosynthesis of NH_4^+ from a Rhenium(V) Nitride. Cyclic voltammetry of a solution of **2** along with 4 equiv of $[HNEt_3][PF_6]$ results in an irreversible wave at the first reduction of **2** with more than three-fold higher current passed (Figure 4). These observations are consistent with multiple rapid chemical and electrochemical reactions occurring after reduction, as might be expected for a series of proton and electron transfers.

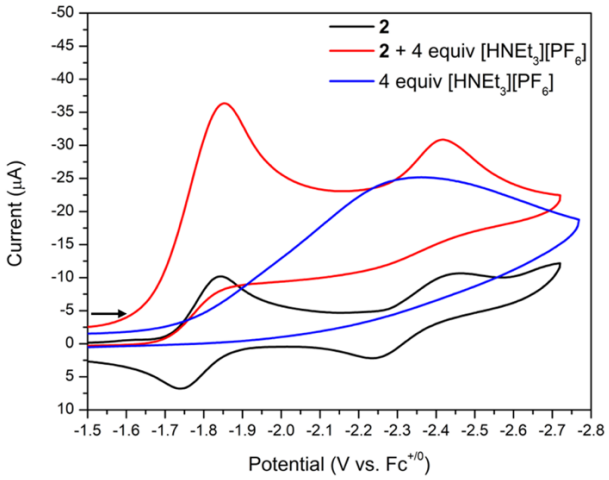

Figure 4. Cyclic voltammograms (100 mV/s) of **2** (black), **2** with four equiv of $[HNEt_3][PF_6]$ added (red), and four equiv of $[HNEt_3][PF_6]$ alone taken in PhF with 0.2 M $[NBu_4][PF_6]$ (blue). Glassy carbon working electrode, $Ag^{+/0}$ reference electrode, Pt wire counter electrode.

Based on these results, controlled potential electrolyses of a mixture of **2** and 4 equiv of $[HNEt_3][PF_6]$ in PhF or THF were performed at a potential of –1.9 V vs. $Fc^{+/0}$. Electrolysis was continued until four electrons per equivalent of **2** had been passed, during which time the solution changed color from light yellow to orange (Scheme 2). $^{31}P\{^1H\}$ NMR analysis of the post-

electrolysis solution confirmed the formation of **3** in approximately 60% spectroscopic yield with respect to the initial concentration of **2**. IC and ^{1}H NMR analyses indicated NH_4^+ yields in the range of 47–74% and Faradaic efficiencies in the range of 35–56% (Table S2). A series of control experiments and ^{15}N labeling experiments verified that the ammonium was derived from the nitride (see Supporting Information).

Scheme 2. Electrosynthesis of Ammonium and **3** via Reduction of **2** with $[HNEt_3][PF_6]$.

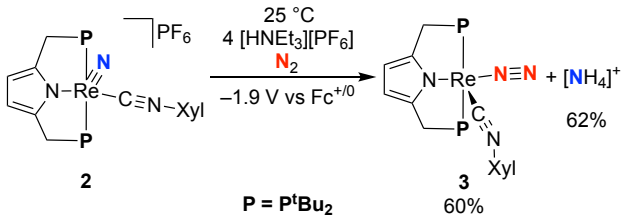

Computational assessment of N–H BDFEs. In order to better characterize PCET to the nitride, we computationally queried the unobserved rhenium(IV) imido complex $[(^{Pyrr}PNP)Re^{IV}(NH)(CNXyl)]^+$ (**4**) product that would come from the first PCET. We used Density Functional Theory (DFT) to estimate the N–H BDFE of **4** in the low-spin doublet state (^{2}**4**), which is expected to be more stable than the high-spin quartet state. All calculations were carried out with a continuum solvent model (THF) using the BP86 functional, the def2-QZVP basis set on rhenium, and def2-TZVP on all other atoms (see SI for details). Using this level of theory, we also calculated the BDFEs for $(^{Pyrr}PNP)Re(NH)Cl$ (^{2}**5**), $(PNP^{tBu})Re(NH)Cl$ (^{2}**6**), and $(PONOP)Re(NH)Cl_2$ (^{2}**7**) for validation and comparison.[45, 50, 58]

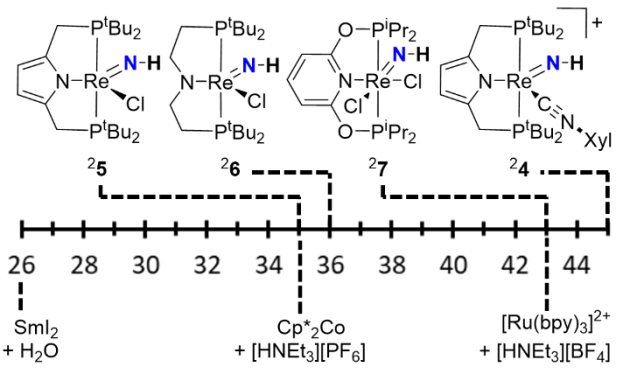

Figure 5. Calculated $N_{nitride}$–H BDFE values (kcal/mol) for a series of related rhenium(IV) imido complexes (above the scale) and the BDFEs of select H-atom donors used in nitrogen reduction (below the scale).

The BDFE values for the $N_{nitride}$–H bonds in ^{2}**7** and ^{2}**6** were calculated to be 43 and 36 kcal/mol, respectively (Figure 5). These values are in good agreement with previous calculations (43 and 33 kcal/mol, respectively).[45, 58] Using this validated method, the BDFE of the N–H bond in ^{2}**5** was calculated to be 35 kcal/mol and that in ^{2}**4** was calculated to be 45 kcal/mol. Thus, replacement of the chloride with isocyanide leads to an impressive 10 kcal/mol increase in the first N–H BDFE, explaining why tuning the redox potential with the isocyanide ligand enables ammonia production. The BDFEs of subsequent N–H bonds are stronger[47] (calculated to be > 60 kcal/mol, see Tables S13-S14) and the CV experiments above suggest that they are formed rapidly to give ammonia. Since ammonia release in this system gives spontaneous binding of N_2, we next explored the N_2 complexes.

Synthesis of a mixed-valent ReNNRe complex with an π^{11} configuration. Complex **3** features a new N_2 ligand, which binds terminally. This binding mode is typical of square pyramidal d^6 metal complexes, which have the same π-bond order in terminal and bridging N_2 binding modes.[40] With respect to the d^5 rhenium(II) needed for a π^{10} configuration in the MNNM complex sought for N_2 splitting, the system is "over-reduced." Therefore, we explored oxidation of **3**.

Complex **3** undergoes an irreversible oxidation, E_{pa} = –0.10 V vs $Fc^{+/0}$ at 100 mV/s (Figure 6) that shifted anodically with higher scan rate, implying that an EC process was occurring. We hypothesized that this involved N_2 dissociation and formation of a dinuclear species by analogy to oxidation of other π^{12} systems.[46]

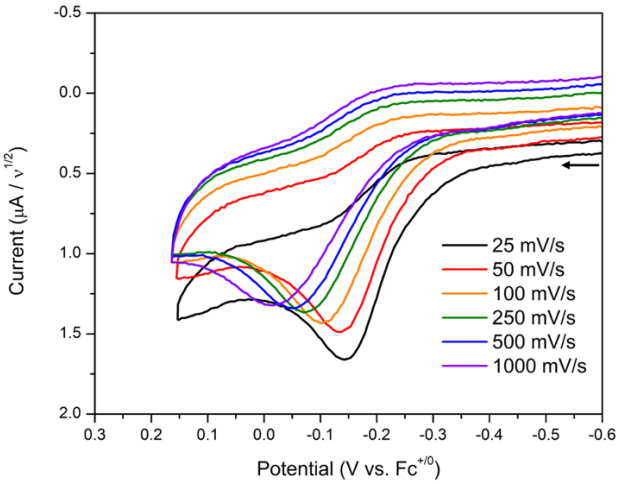

Figure 6. Scan rate dependence of **3**'s first oxidative wave indicating lack of reversibility at fast scan rates. 0.2 M $[NBu_4][PF_6]$ in PhF, glassy carbon working electrode, $Ag^{+/0}$ reference electrode, Pt wire counter electrode. The full voltammogram is shown in Figure S79.

Scheme 3. Synthesis of **8** and **9**.

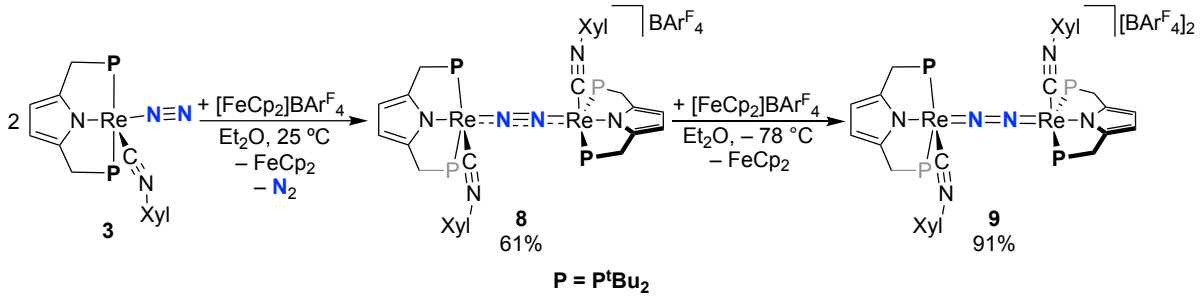

Chemical oxidations of **3** were carried out to test for formation of bridging N_2 complexes. Addition of 1 equiv of $[Fc][BAr^F{}_4]$ (Ar^F = 3,5-bis(trifluoromethyl)phenyl) to an Et_2O solution of **3** at −30 °C gave a 56% yield of **2** after several days at room temperature (Figure S43). The formation of a rhenium nitride product suggests that oxidation indeed induces formation of a bridging N_2

complex that can undergo N_2 cleavage. To identify possible intermediates on the way to **2**, the oxidation of **3** was repeated with only 0.5 equiv of [Fc][BAr^F_4], which resulted in a color change from dark amber to indigo (Scheme 3). A ^{1}H NMR spectrum of the reaction mixture showed the appearance of peaks corresponding to a paramagnetic compound. X-ray diffraction identified this compound as the monocationic N_2-bridged complex {[(^{Pyrr}PNP)Re(CNXyl)]$_2N_2$}[BAr^F_4] (**8**) (Figure 7), which was isolated in 61% yield. The CNXyl remains in the axial position, and the pyrrole unit is *trans* to the N_2 bridge. The N–N bond length is 1.151(8) Å, elongated from 1.121(4) Å in **3** and reflecting the increased weakening of the N–N bond in the π^{11} configuration.[39] The Re–C_{CNXyl} bond lengths are 1.857(9)/1.862(8) Å, the isocyanide N–C bond lengths are 1.229(10)/1.212(9) Å, and the isocyanide C–N–C angles are 144.2(7)/154.6(8)º, indicating a similar amount of backbonding in the two isocyanides of the monocationic complex. The Re–^{pyrr}PNP bond lengths are also similar at the two Re centers, with the largest deviation only 4.7σ.

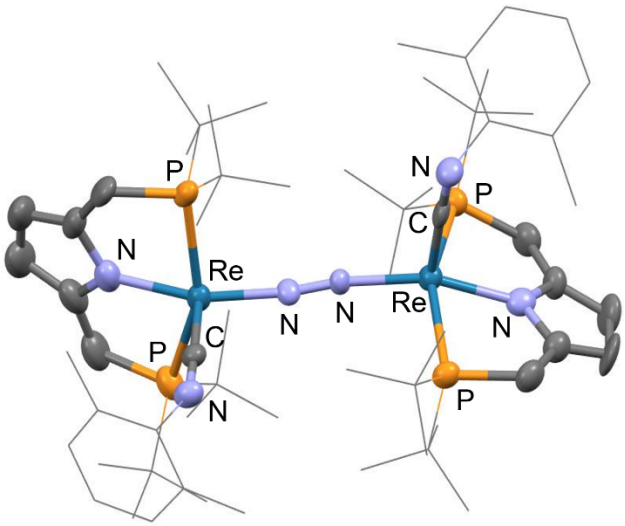

Figure 7. Solid-state structure of complex **8** with thermal ellipsoids at 50% probability. Hydrogen atoms and $BAr^F_4{}^-$ are omitted for clarity.

The Evans method[76] was used to measure the room temperature solution magnetic moment of **8** in CD_2Cl_2 as 1.4 ± 0.2 μ_B, which indicates an $S = 1/2$ ground state (expected 1.7 μ_B). No EPR signal was observed for solutions in CH_2Cl_2 at RT or 10 K (see below). The IR spectrum of **8** displays two broad CNXyl bands at 1925 and 1819 cm^{-1} that do not shift in the $^{15}N_2$ isotopologue, **8–$^{15}N_2$**. DFT calculations suggest that these are attributable to the symmetric and asymmetric combinations of the CNXyl stretching modes, respectively (calculated 1897 and 1856 cm^{-1}) (Table 2). The deviation between the calculated and experimental frequencies of these two CNXyl modes may be due to variation in the relative positioning of the isocyanide ligands between the calculated and solution-phase structures, which could perturb the coupling between the modes and therefore the energy difference between the symmetric and asymmetric bands. Resonance Raman (rR) spectra of frozen solutions (77 K, CH_2Cl_2) of **8** revealed a band at 1799 that shifted to 1739 cm^{-1} in **8–$^{15}N_2$** (calcd for harmonic oscillator = 1738 cm^{-1}), suggestive of a localized N–N stretching mode. An isotopically sensitive band attributable to a localized Re–N vibrational mode was seen in the rR spectra of **8** at 542 cm^{-1}, shifting to 527 cm^{-1} for **8–$^{15}N_2$**) (calcd for harmonic oscillator = 527 cm^{-1}; Figure 8, top).

The lack of IR activity of the N–N vibration and the similar metrical parameters at the two sites suggest the two Re sites are equivalent. The DFT computations show that the SOMO of **8** is part of the MNNM π-manifold and has spin density evenly spread over both rhenium centers (Figure 9). Each of these indicate full electron delocalization across both sites (Robin-Day class III). We tested this idea further by analyzing the near-IR spectrum of **8**, which showed bands at 866 nm (11550 cm^{-1}) and 1194 nm (8374 cm^{-1}) that are consistent with intervalence charge transfer (IVCT) transitions. The peak widths (Figure S63) suggest that λ is near unity,[77-78] as expected for a class III mixed-valence system. The delocalization of the unpaired electron across

the ReNNRe core of **8** may contribute to rapid relaxation of the unpaired spin, which would broaden the EPR signal and may explain why it is not observed (see above).

Table 2. Comparison of **8** and **9**. Frequencies in cm^{-1}, distances in Å, angles in deg. Distances and angles are given as averages of the two sides of the molecule, with the range in parentheses.

	8(exp)	**8**(calcd) $S = 1/2$	**9**(exp)	**9**(calcd) $S = 1$	**9**(calcd) $S = 0$
ν_{N-N}	1799	1821	1701	1760	1759
ν_{C-N}	1819	1856	1990	1992	1925
ν_{C-N}	1925	1897	2031	2013	1979
ν_{Re-N}	542	610	556	641	634, 645
N–N	1.151(8)		1.151(9)		
Re–N (N_2)	1.97(1)		1.94(1)		
Re–C	1.86(1)		1.94(1)		
C–N (isocyanide)	1.22(1)		1.17(1)		
N–Re–N	161(1)		169(6)		
C–Re–N	100(2)		93(8)		
C–N–C (isocyanide)	150(6)		163(1)		

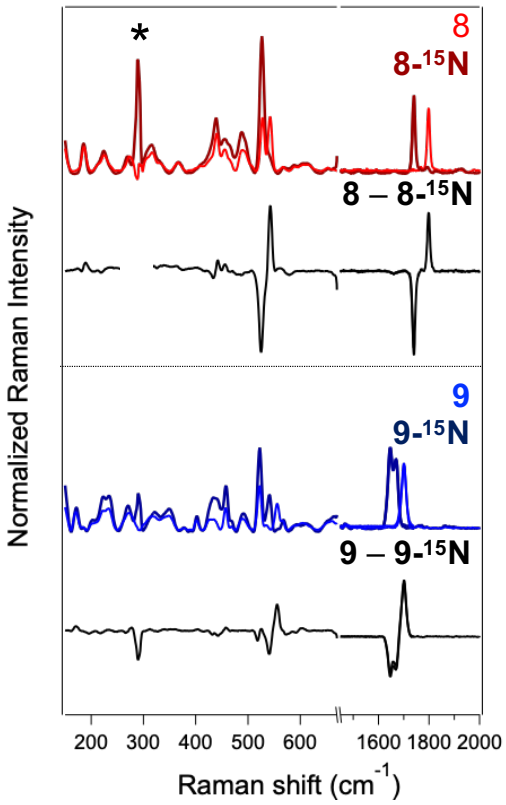

Figure 8. Resonance Raman spectra (λ_{ex} = 568 nm; power = 15 mW; 77 K; in CH_2Cl_2) of **8**, **8**–$^{15}N_2$, **9**, and **9**–$^{15}N_2$**.** Direct subtractions of the two spectra are shown below each pair. Residual signal from CD_2Cl_2 solvent is indicated with an asterisk (*).

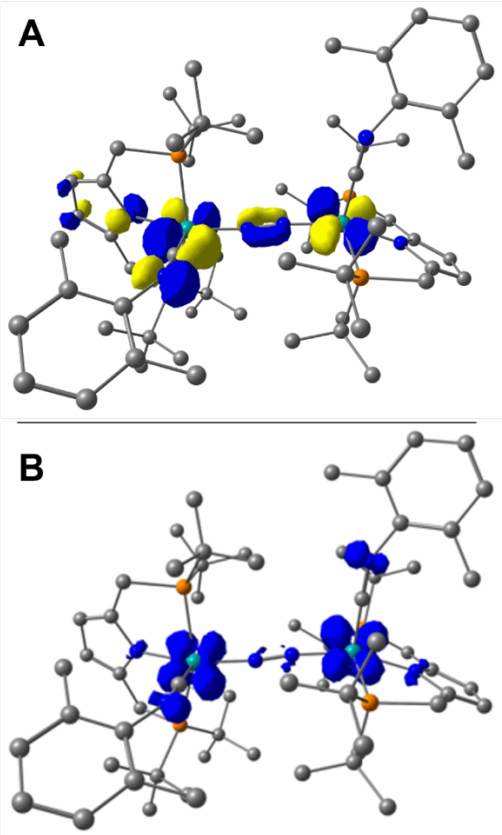

Figure 9. Kohn-Sham SOMO (A) and spin-density plot for **8** (B) displayed at contour values of 0.05 and 0.005 a.u., respectively.

Oxidation to a ReNNRe species with a π^{10} configuration. Complex **8** has a π^{11} configuration, so it requires one-electron oxidation to reach a π^{10} configuration that would be predicted to initiate N_2 splitting.[38-40] CV of **8** in PhF showed a quasi-reversible oxidation at –0.24 V vs $Fc^{+/0}$ for which the $i_{p,a}/i_{p,c}$ ratio becomes larger at slower scan rates (Figure S84), suggesting that the oxidation is followed by a chemical reaction. We explored this phenomenon through chemical oxidation. Adding 1 equiv of [Fc][BAr^F_4] to a Et_2O solution of **8** at –78 °C generated the oxidation product, {[(^{Pyrr}PNP)Re(CNXyl)]$_2$$N_2$}[$BAr^F_4$]$_2$ (**9**) (Scheme 3). NMR spectroscopy including ^{1}H–^{31}P HMBC suggest that there is hindered rotation about the Re–N–N–Re axis (see Supporting Information). All NMR spectra of **9** display partial formation of the nitride product

that results from N_2 splitting, and oxidation of **8** at room temperature results in a greater fraction of nitride in the product mixture.

The crystal structure of **9** (Figure 10) is notable, as there are few examples of isolable π^{10} MNNM complexes that spontaneously undergo N_2 splitting.[13] The N–N bond length is 1.151(9) Å and the Re–N_{N2} bond lengths are 1.948(7) and 1.936(7) Å. The Re–C_{CNXyl} bond lengths are 1.941(11) and 1.938(10) Å, the isocyanide N–C bond lengths are 1.173(13) and 1.164(13) Å, and the isocyanide C–N–C angles are 163.2(10) and 157.6(10)º, all indicating less π-backbonding into the isocyanide ligand than in **8**. This agrees with the IR spectra of **9**, which shows higher C–N stretching frequencies (overlapping bands at 2031 and 1990 cm^{-1} assigned as the symmetric and asymmetric combination bands) than in **8**.

The rR spectrum of **9** (77 K, CH_2Cl_2) shows an intense band at 1701 cm^{-1} (apparent Fermi doublet at 1646/1669 cm^{-1} for **9–$^{15}N_2$**) that is assigned to the N–N stretching mode (DFT calculated 1643 cm^{-1}). This vibrational mode is shifted to lower energy relative to the analogous mode in **8**. Another band at 556 cm^{-1} (539 cm^{-1} for **9–$^{15}N_2$**) was assigned as a local Re–N stretching vibration (Figure 8, bottom). Notably, this band is shifted to higher energy relative to the Re-N stretching mode in **8**. Though these oppose the trend typically expected for backbonding from metals in different oxidation states, these shifts (and the change in the Re–N bond distances noted above) agree with the depopulation of a MNNM orbital with Re–N π-antibonding character going from π^{11} complex **8** to π^{10} complex **9** (Figure 1 above). Thus they are neatly explained using the delocalized MO model of the MNNM core.[39]

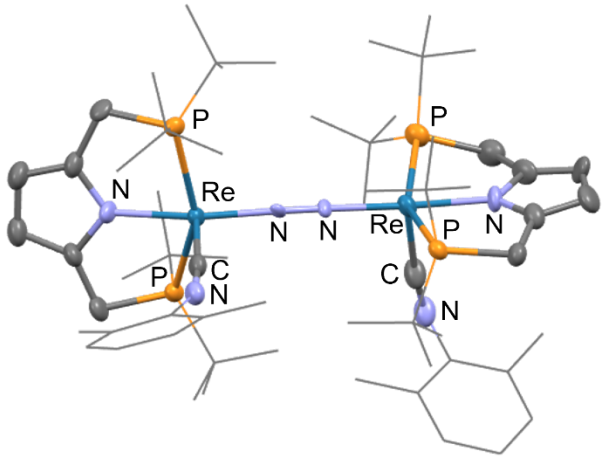

Figure 10. Solid-state structure of complex **9** with thermal ellipsoids at 50% probability. Hydrogen atoms and $BAr^F{}_4^-$ anions are omitted for clarity.

N_2 Splitting. Complex **9** has the correct π^{10} configuration for N_2 splitting, which corresponds to a total N–N bond order of 2.[39-40] Heating a CD_2Cl_2 solution of **9** to 40 °C for one hour resulted in a color change from purple to yellow-brown, and the ^1H and $^{31}P\{^1H\}$ NMR spectra of this solution showed that N_2 had split to give the nitride species **2** in 93% spectroscopic yield (Scheme 4).

Scheme 4. N_2 Splitting From **9**

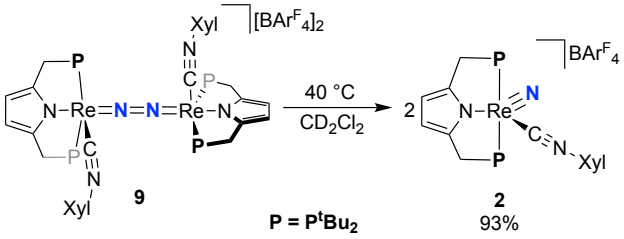

In an effort to further understand the electronic structure of **9** and the N_2 splitting mechanism, we turned to DFT using the same protocol described above. We optimized the geometry of **9** in the singlet (^{1}**9**), triplet (^{3}**9**), and open shell singlet (^{OS1}**9**) states. The triplet ^{3}**9** was lowest in energy, but ^{OS1}**9** was only 2 kcal/mol higher in energy. ^{1}**9** was calculated to be higher in

energy than ^{3}**9** by 6–7 kcal/mol, with the *caveat* that hybrid functionals often favor high-spin states.[79] Direct splitting from ^{3}**9** to give **2** is 7 kcal/mol downhill, but the lowest-energy transition state (^{1}**9-TS**) has a huge barrier of 52 kcal/mol (Figure 11).

In order to resolve this issue, we next considered a rotamer **9'**, where the planes of the ^{Pyrr}PNP ligands have rotated to leave vacant coordination sites *trans* to the Re–N–N–Re core. The relative spin-state energetics are similar, but ^{3}**9'** is 18 kcal/mol uphill from ^{3}**9**, explaining why this rotamer is not observed experimentally. Importantly, the barrier to N–N cleavage from ^{3}**9'** is only 14 kcal/mol over the singlet transition state ^{1}**9'-TS**, which has the familiar zigzag geometry.[41-42] We were unable to converge the structures for the isomerization transition states (see Supporting Information), but if this barrier is relatively low then the formation of the rotamer could explain the facile N–N splitting.

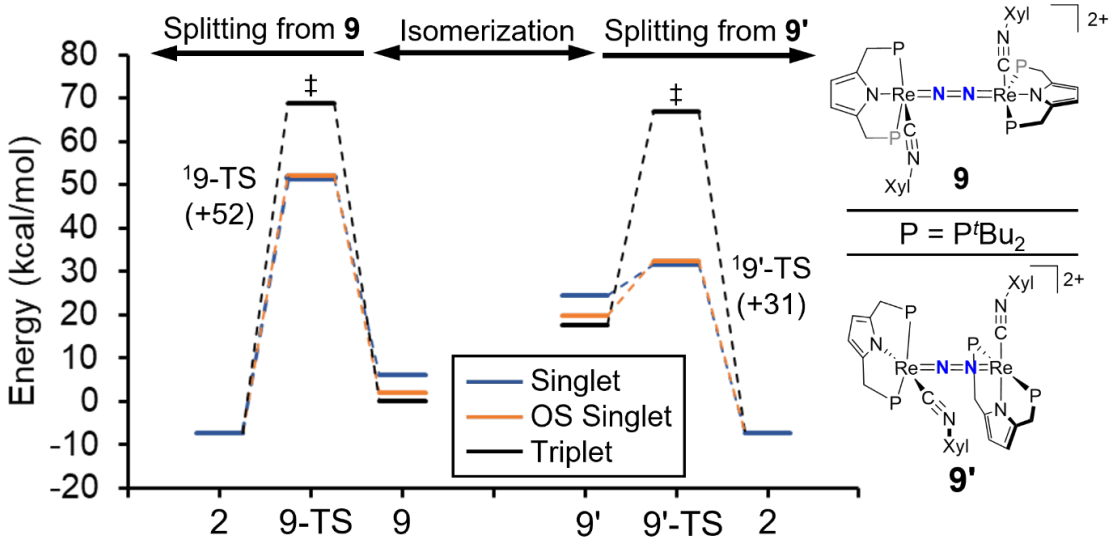

Figure 11. Calculated potential energy surfaces for N_2 splitting from **9** and **9'** to **2**. Energies are set relative to ^{3}**9**. The geometries of the rotamers are shown on the right.

A key step during the N_2-splitting reaction is the thermal accessibility of a σ-symmetry orbital that is collinear with the Re–N–N–Re core and σ* in character with respect to the N–N bond.[39] The energy of this orbital is related to the presence or absence of a ligand in the positions *trans* to the Re–N–N–Re core.[44-45] For ^{3}**9**, this orbital was found at α-LUMO+10, while in ^{3}**9'** this orbital is the α-LUMO. (Diagrams of the frontier orbitals of **9**, **9'**, and the relevant transition states are given in the Supporting Information.) This suggests that the N–N σ* orbital for ^{3}**9** becomes more accessible in the rotamer ^{3}**9'**, due to the lack of a ligand *trans* to the N_2 unit.[38] This enables the key N–N bond splitting to take place, but heating is required to access the less-favored rotamer.

Discussion

Electrosynthesis of NH_4^+ from 2. It is important that the nitrido ligand of **2** can be electrochemically converted to NH_3. Few reports have demonstrated electrochemical N_2 reduction and fewer yet have demonstrated this transformation catalytically.[24, 30, 80-86] A seminal report from Pickett and coworkers found that *trans*-$(dppe)_2W(N_2)_2$ was capable of N_2 reduction to 0.23 equiv of NH_3 at –2.6 V vs. $Fc^{+/0}$ in THF using tosylic acid.[83] In contrast, we electrolyzed **2** at a less cathodic potential of –1.8 to –1.9 V vs. $Fc^{+/0}$ using $[HNEt_3][PF_6]$, a milder acid with a pK_a of 12.5 in THF. Nitrides are likely involved in state-of-the-art homogenous electrocatalysis with PCET mediators, such as an Fe system that produces 2.6 equiv of NH_3 at –2.1 V vs. $Fc^{+/0}$ in Et_2O at –35 °C with 50 equiv of $[H_2NPh_2][BAr^F{}_4]$ (pK_a = 3.2 in THF),[80] and an Mo system that gives 4.7 equiv of NH_3 at –1.9 V vs. $Fc^{+/0}$ in THF at room temperature with 1000 equiv of collidinium triflate (pK_a = 8.1 in THF).[24] Beyond these examples, which invoke nitride intermediates, we are not aware of examples of ammonia synthesis via electroreduction of an N_2-derived nitride complex.

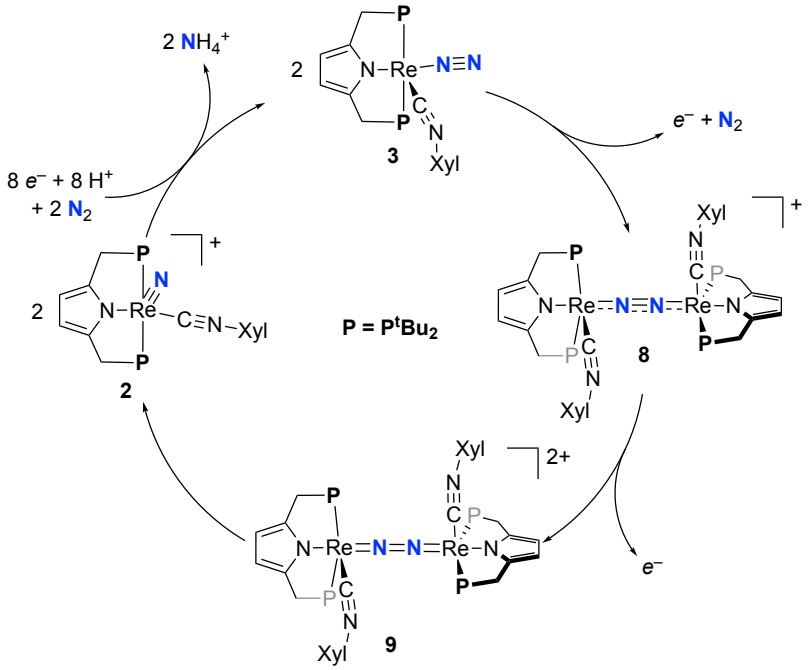

Scheme 5. Synthetic Cycle for the Conversion of N_2 to NH_4^+ Using the (^{Pyrr}PNP)Re(CNXyl) System

Scheme 5 shows how this production of NH_4^+ fits into a synthetic cycle for ammonia formation from N_2. The drawback to the system described here is that the rhenium species **3** that results from ammonia production is over-reduced: it needs to be oxidized to **9** in order to undergo N–N bond splitting. Other rhenium systems that suffered from over-reduction could be 'rescued' under electrochemical conditions by oxidation with a Re^{III} species (comproportionation), resulting in the correct oxidation states for N_2 splitting.[47, 87] With the electrolysis of **2**, the metal species that predominate in solution are the Re^{V} complex **2** and the Re^{I} complex **3**, and the intermediates speedily proceed to ammonia. The putative Re^{III} analogues that might 'rescue' **3** back to the Re^{II} oxidation state required for splitting (*e.g.* Re–N–H_x) have low concentrations, and they are presumably reduced before they can undergo comproportionation. In the future, it may be possible to design new systems (*e.g.* alternating polarization or photoredox catalysis) to reduce and oxidize

in the same solution, benefitting from the mild conditions for electrochemical generation of NH_3 in this system.

Isolation of N_2 complexes with π^{11} and π^{10} cores. In this system, we were also able to isolate discrete steps along the N_2 binding and splitting pathway, allowing for study of the electronic structures of intermediate metal-N_2 complexes. The present Re system is noteworthy for having MNNM species that are isolable in *both* of the elusive π^{11} and π^{10} states.[13, 36, 47, 49] One important observation is that the oxidation of the terminal N_2 complex **3** to the bridging N_2 complex **8** is qualitatively slower (hours) than the oxidation of bridging **8** to bridging **9** (minutes), indicating that bridge formation may indeed be slow in oxidative N_2 splitting systems. Previously, *trans*-$Mo(depe)_2(N_2)_2$ was reported to form a terminal nitride from N_2 upon oxidation by $[Fc][BAr^F{}_4]$ (or electrolysis at E^o = +0.5 V vs. Pt wire), and it was proposed based on UV-visible spectroelectrochemistry and DFT computations that the rate-limiting step was N_2 loss prior to formation of the MNNM complex.[46] In complementary work, computations by Arashiba *et al.* indicate a substantial barrier to dissociation of terminal N_2 ligands *after* an N_2 bridge is formed.[88]

In this work, the path to N_2 cleavage starts from terminal Re^I–N_2 complex **3**, which is "over-reduced." As expected from the π-orbital model in Figure 1, it must be oxidized to give a bridging N_2 complex, and further oxidized to split N_2.[39-40] Oxidative N_2 splitting is rare, but has been observed in a few systems. For example, the π^{12} complex $[(^{py}PNP)Mo(N_2)_2]_2(\mu\text{-}N_2)$ performs N_2 splitting through chemical oxidation or comproportionation with more oxidized species in solution.[87] We have also analyzed electrochemical N_2 reduction mechanisms, and concluded that oxidation of an over-reduced Re^I-N_2 complex by a Re^{III} species) is an important step.[47, 49] In the system described here, we attempted to electrochemically oxidize **3** to **8** but this was unsuccessful,

possibly due to the more rapid formation of unstable intermediates on the timescale of the electrochemical experiment (see Supporting Information).

The ability to isolate the π^{11} complex **8** enables characterization of a rare mixed-valence complex of N_2. The lack of IR activity of the N_2 stretching mode, the metrical parameters, and analysis of the IVCT band each indicate that the valence is fully delocalized. Class III behavior was also found in an amide-supported MoNNMo system with a π^{11} core.[89] The related π^{11} coordination polymer $[K(N_2)\{(^{Pyrr}PNP)Mo(N_2)\}_2]_n$ was recently reported and similarly does not split N_2.[90] Finally, the π^{11} diosmium complex $[(NH_3)_5Os]_2(\mu\text{-}N_2)^{5+}$ splits N_2 with photolysis,[91-94] which has been evaluated computationally.[95]

Further oxidation gives a π^{10} system **9**, in which the N–N bond is weakened as expected from the π-orbital model. It has the correct configuration for N_2 splitting, but N_2 splitting is slow at room temperature which contrasts with most such systems.[13, 88, 96] We propose that the sluggish N_2 cleavage from **9** results from the unfavorable orientation of the pincer ligands with respect to the Re–N–N–Re core. In the ground-state conformation **9** has a ligand *trans* to MNNM, which raises the energy of the σ* orbital that must be populated for N_2 splitting. Our DFT computations indicate that rotation of the ligands leads to a more productive conformer where the *trans* positions are vacant. The rotated conformer ^{3}**9'** is calculated to be 18 kcal/mol uphill from ^{3}**9**, but it can split N_2 through a transition state that is 20 kcal/mol lower in energy than the transition state starting from **9**, because the MNNM σ* orbital has become the LUMO in ^{3}**9'**. Thus, the slowness of N–N cleavage to the nitride complex **2** results mostly from the activation barrier for rotation. Rapid N_2 cleavage requires a molecular design that gives a conformation with no donor *trans* to the bridging N_2.[38,44-45]

Benefits of isocyanide as a second supporting ligand. The most important difference between **2** and the other N_2-splitting-derived rhenium nitrides[45, 47, 49-51, 62, 97] is the milder reduction potential and the reversibility of observed CV waves in the absence of protons. One advantage is that the relatively mild potential minimizes parasitic H_2 production. It is also crucial to consider the BDFE for the first N–H bond formed from the nitride[58] (see Figure 5 above). The isocyanide-bearing complex **4** has a relatively high calculated N–H BDFE of 45 kcal/mol, which is much stronger than the chloride analogue **5** (35 kcal/mol). The large difference can be attributed to the dramatic >1.4 V change in the $Re^{V/IV}N$ reduction potential from switching the anionic chloride to the neutral, π-accepting isocyanide. According to eq 1, this is equivalent to a difference of >32 kcal/mol in N–H BDFE (in the absence of a change of pK_a).[27, 60] Often, the change in BDFE from shifting the redox potential of a system is compensated by a shift in the pK_a, resulting in little net change to the BDFE.[27, 98-100] The calculated 10 kcal/mol difference between BDFE values in **4** and **5** indicates that in this system, the pK_a does not fully compensate for the dramatic change in the reduction potential, contributing to the ability of **2** to convert the nitride ligand to ammonia. Considering recent results on PCET, we suggest that this lack of adherence to the expected compensating relationship could result from the delocalization of the charge transfer onto the isocyanide unit, which is distant from the protonation site on the nitride and thus separates the protonation and reduction sites.[101] In any case, we demonstrate here that isocyanide as a secondary supporting ligand benefits ammonia formation.

The π-accepting nature of the isocyanide also contributes to the structure and physical properties of the species observed in the synthetic cycle in Scheme 5. Complex **3** has a terminal N_2 ligand, as predicted from Hasanayn's "π-bond order" model for a square pyramidal complex with a d^6 configuration.[40] This contrasts with the bridging N_2 ligand in $\{(^{py}PNP)ReCl(N_2)\}_2(\mu$-

N_2),[51] a π^{12} system. Backbonding into isocyanide is clearly indicated by the decrease of the C–N–C_{Xyl} angle and elongation of the C≡N_{Xyl} bond from free CNXyl, and probably is the reason for the anomalously broad C–N stretching bands in the IR spectra.[102-104]

Though this backbonding facilitates reduction of the nitride as part of ammonia formation, it also facilitates over-reduction to the formal rhenium(I) level. This over-reduction necessitates oxidation of terminal N_2 complex **3** to initially form bimetallic **8**, which has formal $Re^{I}Re^{II}$ character. The bonding metrics in **8** are quite similar to those in **3**, but the symmetric stretching band of the isocyanides in **8** is higher by 118 cm^{-1} relative to **3**, indicating some lessening in isocyanide backbonding with oxidation. Further oxidation from **8** to **9** results in elongation of the Re–C bonds and shifting of the C≡N_{Xyl} stretching modes to higher frequencies by 100-200 cm^{-1}. All of these changes indicate that the rhenium centers in **9** are more weakly backbonding to the π* orbitals of the CNXyl ligands than in those in **8**. The bridging N_2 ligand responds in the opposite way, with oxidation of **3** to **8** resulting in a decrease in the N_2 stretching frequency by 197 cm^{-1} and further oxidation to **9** decreasing the frequency by another 98 cm^{-1}. This can be attributed to the delocalized nature of the bonding in the ReNNRe core (see previous section, and MOs in Figure 1),[39] and indicates that the ReNNRe bonding should not be considered with the typical backbonding model.[37] Future work will explore the influences of isocyanides on the multiple accessible redox levels of these rhenium complexes, with particular attention to facilitating PCET reduction of nitride without over-reduction to rhenium(I).

Conclusions

Complex **2** is a rare example of an N_2-derived nitride that can form ammonia both chemically and electrochemically using a weak acid at ambient temperature and pressure. This

was accomplished by replacing chloride with the π-accepting, neutral xylyl isocyanide, which lessens the cathodic potential for nitride reduction. This change increases the BDFE of the first N–H bond and is *not* fully counteracted by a change in pK_a, and the decoupling of potential and pK_a enables the production of ammonia. This system provides additional insight because it is possible to crystallographically characterize many intermediates in the pathway from N_2 to ammonia. Complex **3** is the rhenium-containing product of nitride reduction and is "over-reduced" from the perspective of N_2 splitting. Upon oxidation of **3**, an N_2-bridged species **8** forms which has a π^{11} configuration and is fully valence-delocalized (class III). Complex **8** can be oxidized to give the π^{10} complex **9**. This complex has the correct electron configuration for splitting N_2 and does so after rotation of the supporting ^{Pyrr}PNP ligand.

Because the nitride can be regenerated via splitting of N_2, the system reported here demonstrates a synthetic cycle for the conversion of N_2 to NH_4^+ through the nitrido species **2**. Overall, this work describes geometric and electronic tuning strategies for successful generation of ammonia from N_2. More generally, we suggest that the incorporation of a second, π-accepting supporting ligand may be a useful tactic for enhancing the ability of various N_2-splitting systems to navigate the various steps from N_2 to ammonia.

Supporting Information

The Supporting Information is available free of charge at XXXXX.

Synthetic details, spectra, and computational details (PDF)

Crystallographic information (CIF)

Coordinates from computations (XYZ)

Accession Codes

CCDC 2358089-2358092 contain the supporting crystallographic data for this paper. These data can be obtained free of charge via www.ccdc.cam.ac.uk/data_request/cif, by emailing data_request@ccdc.cam.ac.uk, or by contacting The Cambridge Crystallographic Data Centre, 12 Union Road, Cambridge CB2 1EZ, UK; fax: +44 1223 336033.

Corresponding Authors

Hannah S. Shafaat, Department of Chemistry and Biochemistry, University of California, Los Angeles, CA, shafaat@ucla.edu

Alexander J. M. Miller, Department of Chemistry, University of North Carolina, Chapel Hill, NC, ajmm@email.unc.edu

Patrick L. Holland, Department of Chemistry, Yale University, New Haven, CT, patrick.holland@yale.edu

Author Contributions

J.E.W., N.D.M., and A.S.H. contributed equally to performing experiments, interpreting data, and writing the manuscript, and are considered co-first authors.

M.A. performed supplementary electrochemical experiments, A.E.W. performed resonance Raman experiments and interpreted data, and B.Q.M. solved X-ray crystal structures. R.H.C., H.S.S., A.J.M.M. and P.L.H. provided supervision and edited the paper.

Conflicts of Interest

The authors declare no competing financial interest.

Acknowledgments

This work was supported by the U.S. National Science Foundation (CHE-2247258 to P.L.H., CHE-2247259 to A.J.M.M., DGE-1752134 to J.E.W., CHE-2108684/CHE-2419343 to H.S.S.). We thank Profs. Alan Goldman and James Mayer for helpful discussions.

Graphical Abstract

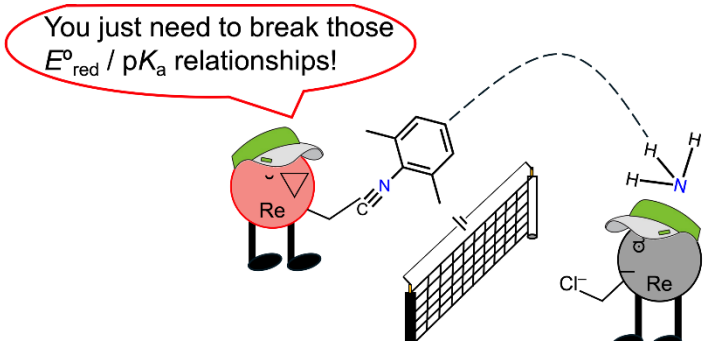

References

1. Smil, V., Global Population and the Nitrogen Cycle. *Sci. Am.* **1997,** *277*, 76–81.
2. Jennings, J. R., *Catalytic ammonia synthesis, fundamentals and practice*. Plenum Press: New York, 1991.
3. Erisman, J. W.; Sutton, M. A.; Galloway, J.; Klimont, Z.; Winiwarter, W., How a century of ammonia synthesis changed the world. *Nat. Geosci.* **2008,** *1*, 636-639.
4. Schlögl, R., Catalytic Synthesis of Ammonia—A "Never-Ending Story"? *Angew. Chem., Int. Ed.* **2003,** *42*, 2004-2008.
5. Chen, J. G.; Crooks, R. M.; Seefeldt, L. C.; Bren, K. L.; Bullock, R. M.; Darensbourg, M. Y.; Holland, P. L.; Hoffman, B.; Janik, M. J.; Jones, A. K.; Kanatzidis, M. G.; King, P.; Lancaster, K. M.; Lymar, S. V.; Pfromm, P.; Schneider, W. F.; Schrock, R. R., Beyond fossil fuel–driven nitrogen transformations. *Science* **2018,** *360*, eaar6611.
6. Jewess, M.; Crabtree, R. H., Electrocatalytic Nitrogen Fixation for Distributed Fertilizer Production? *ACS Sustain. Chem. Eng.* **2016,** *4*, 5855-5858.
7. Shipman, M. A.; Symes, M. D., Recent progress towards the electrosynthesis of ammonia from sustainable resources. *Catal. Today* **2017,** *286*, 57-68.
8. Martín, A. J.; Shinagawa, T.; Pérez-Ramírez, J., Electrocatalytic Reduction of Nitrogen: From Haber-Bosch to Ammonia Artificial Leaf. *Chem* **2019,** *5*, 263-283.
9. Hochman, G.; Goldman, A. S.; Felder, F. A.; Mayer, J. M.; Miller, A. J. M.; Holland, P. L.; Goldman, L. A.; Manocha, P.; Song, Z.; Aleti, S., Potential Economic Feasibility of Direct Electrochemical Nitrogen Reduction as a Route to Ammonia. *ACS Sustain. Chem. Eng.* **2020,** *8*, 8938-8948.
10. Guo, W.; Zhang, K.; Liang, Z.; Zou, R.; Xu, Q., Electrochemical nitrogen fixation and utilization: theories, advanced catalyst materials and system design. *Chemical Society Reviews* **2019,** *48*, 5658-5716.

11. Chanda, D.; Xing, R.; Xu, T.; Liu, Q.; Luo, Y.; Liu, S.; Tufa, R. A.; Dolla, T. H.; Montini, T.; Sun, X., Electrochemical nitrogen reduction: recent progress and prospects. *Chemical Communications* **2021,** *57*, 7335-7349.
12. Chen, Z.; Liu, C.; Sun, L.; Wang, T., Progress of Experimental and Computational Catalyst Design for Electrochemical Nitrogen Fixation. *ACS Catal.* **2022,** *12*, 8936-8975.
13. Forrest, S. J. K.; Schluschaß, B.; Yuzik-Klimova, E. Y.; Schneider, S., Nitrogen Fixation via Splitting into Nitrido Complexes. *Chem. Rev.* **2021,** *121*, 6522-6587.
14. Lin, S.; Zhang, X.; Chen, L.; Zhang, Q.; Ma, L.; Liu, J., A review on catalysts for electrocatalytic and photocatalytic reduction of N2 to ammonia. *Green Chem.* **2022,** *24*, 9003-9026.
15. Pang, Y.; Su, C.; Jia, G.; Xu, L.; Shao, Z., Emerging two-dimensional nanomaterials for electrochemical nitrogen reduction. *Chem. Soc. Rev.* **2021,** *50*, 12744-12787.
16. Ravi, M.; Makepeace, J. W., Facilitating green ammonia manufacture under milder conditions: what do heterogeneous catalyst formulations have to offer? *Chem. Sci.* **2022,** *13*, 890-908.
17. Tian, Y.; Liu, Y.; Wang, H.; Liu, L.; Hu, W., Electrocatalytic Reduction of Nitrogen to Ammonia in Ionic Liquids. *ACS Sustain. Chem. Eng.* **2022,** *10*, 4345-4358.
18. Chalkley, M. J.; Drover, M. W.; Peters, J. C., Catalytic N2-to-NH3 (or -N2H4) Conversion by Well-Defined Molecular Coordination Complexes. *Chemical Reviews* **2020,** *120*, 5582-5636.
19. Tanabe, Y.; Nishibayashi, Y., Catalytic Nitrogen Fixation Using Well-Defined Molecular Catalysts under Ambient or Mild Reaction Conditions. *Angewandte Chemie International Edition* **2024,** *63*, e202406404.
20. Yandulov, D. V.; Schrock, R. R., Catalytic Reduction of Dinitrogen to Ammonia at a Single Molybdenum Center. *Science* **2003,** *301*, 76-78.
21. Schrock, R. R., Catalytic Reduction of Dinitrogen to Ammonia at a Single Molybdenum Center. *:Acc. Chem. Res.* **2005,** *38*, 955-962.
22. Arashiba, K.; Miyake, Y.; Nishibayashi, Y., A molybdenum complex bearing PNP-type pincer ligands leads to the catalytic reduction of dinitrogen into ammonia. *Nat. Chem.* **2011,** *3*, 120-125.
23. Nishibayashi, Y., Recent Progress in Transition-Metal-Catalyzed Reduction of Molecular Dinitrogen under Ambient Reaction Conditions. *Inorg. Chem.* **2015,** *54*, 9234-9247.
24. Ibrahim, A. F.; Garrido-Barros, P.; Peters, J. C., Electrocatalytic Nitrogen Reduction on a Molybdenum Complex Bearing a PNP Pincer Ligand. *ACS Catalysis* **2023,** *13*, 72-78.
25. Ashida, Y.; Arashiba, K.; Nakajima, K.; Nishibayashi, Y., Molybdenum-catalysed ammonia production with samarium diiodide and alcohols or water. *Nature* **2019,** *568*, 536-540.
26. Ashida, Y.; Mizushima, T.; Arashiba, K.; Egi, A.; Tanaka, H.; Yoshizawa, K.; Nishibayashi, Y., Catalytic production of ammonia from dinitrogen employing molybdenum complexes bearing N-heterocyclic carbene-based PCP-type pincer ligands. *Nature Synthesis* **2023,** *2*, 635-644.
27. Agarwal, R. G.; Coste, S. C.; Groff, B. D.; Heuer, A. M.; Noh, H.; Parada, G. A.; Wise, C. F.; Nichols, E. M.; Warren, J. J.; Mayer, J. M., Free Energies of Proton-Coupled Electron Transfer Reagents and Their Applications. *Chem. Rev.* **2022,** *122*, 1-49.
28. Warren, J. J.; Tronic, T. A.; Mayer, J. M., Thermochemistry of Proton-Coupled Electron Transfer Reagents and its Implications. *Chem. Rev.* **2010,** *110*, 6961-7001.

29. Weinberg, D. R.; Gagliardi, C. J.; Hull, J. F.; Murphy, C. F.; Kent, C. A.; Westlake, B. C.; Paul, A.; Ess, D. H.; McCafferty, D. G.; Meyer, T. J., Proton-Coupled Electron Transfer. *Chem. Rev.* **2012,** *112*, 4016-4093.
30. Garrido-Barros, P.; Derosa, J.; Chalkley, M. J.; Peters, J. C., Tandem electrocatalytic N2 fixation via proton-coupled electron transfer. *Nature* **2022,** *609*, 71-76.
31. Ashida, Y.; Onozuka, Y.; Arashiba, K.; Konomi, A.; Tanaka, H.; Kuriyama, S.; Yamazaki, Y.; Yoshizawa, K.; Nishibayashi, Y., Catalytic nitrogen fixation using visible light energy. *Nature Communications* **2022,** *13*, 7263.
32. Johansen, C. M.; Boyd, E. A.; Peters, J. C., Catalytic transfer hydrogenation of N2 to NH3 via a photoredox catalysis strategy. *Science Advances* **2022,** *8*, eade3510.
33. Burgess, D. R., *NIST Chemistry WebBook*. National Institute of Standards and Technology: Gaithersburg, MD, 2017.
34. Kim, S.; Park, Y.; Kim, J.; Pabst, T. P.; Chirik, P. J., Ammonia synthesis by photocatalytic hydrogenation of a N2-derived molybdenum nitride. *Nat. Synth.* **2022,** *1*, 297-303.
35. Klopsch, I.; Yuzik-Klimova, E. Y.; Schneider, S., Functionalization of N2 by Mid to Late Transition Metals via N–N Bond Cleavage. In *Nitrogen Fixation*, Nishibayashi, Y., Ed. Springer International Publishing: Cham, 2017; pp 71-112.
36. Singh, D.; Buratto, W. R.; Torres, J. F.; Murray, L. J., Activation of Dinitrogen by Polynuclear Metal Complexes. *Chem. Rev.* **2020,** *120*, 5517-5581.
37. Weber, J. E.; Bhutto, S. M.; Genoux, A. T. Y.; Holland, P. L., 1.17 - Dinitrogen Binding and Functionalization. In *Comprehensive Organometallic Chemistry IV*, Parkin, G.; Meyer, K.; O'hare, D., Eds. Elsevier: Oxford, 2022; pp 521-554.
38. Bruch, Q. J.; Connor, G. P.; McMillion, N. D.; Goldman, A. S.; Hasanayn, F.; Holland, P. L.; Miller, A. J. M., Considering Electrocatalytic Ammonia Synthesis via Bimetallic Dinitrogen Cleavage. *ACS Catal.* **2020,** *10*, 10826-10846.
39. Hasanayn, F.; Holland, P. L.; Goldman, A. S.; Miller, A. J. M., Lewis Structures and the Bonding Classification of End-on Bridging Dinitrogen Transition Metal Complexes. *J. Am. Chem. Soc.* **2023,** *145*, 4326-4342.
40. Yamout, L. S.; Ataya, M.; Hasanayn, F.; Holland, P. L.; Miller, A. J. M.; Goldman, A. S., Understanding Terminal versus Bridging End-on N2 Coordination in Transition Metal Complexes. *J. Am. Chem. Soc.* **2021,** *143*, 9744-9757.
41. Cui, Q.; Musaev, D. G.; Svensson, M.; Sieber, S.; Morokuma, K., N2 Cleavage by Three-Coordinate Group 6 Complexes. W(III) Complexes Would Be Better Than Mo(III) Complexes. *J. Am. Chem. Soc.* **1995,** *117*, 12366-12367.
42. Laplaza, C. E.; Johnson, M. J. A.; Peters, J.; Odom, A. L.; Kim, E.; Cummins, C. C.; George, G. N.; Pickering, I. J., Dinitrogen Cleavage by Three-Coordinate Molybdenum(III) Complexes: Mechanistic and Structural Data. *J. Am. Chem. Soc.* **1996,** *118*, 8623-8638.
43. Neyman, K. M.; Nasluzov, V. A.; Hahn, J.; Landis, C. R.; Rösch, N., Density Functional Study of N2 Activation by Molybdenum(III) Complexes. Unusually Strong Relativistic Effects in 4d Metal Compounds. *Organometallics* **1997,** *16*, 995-1000.
44. Schendzielorz, F.; Finger, M.; Abbenseth, J.; Würtele, C.; Krewald, V.; Schneider, S., Metal-Ligand Cooperative Synthesis of Benzonitrile by Electrochemical Reduction and Photolytic Splitting of Dinitrogen. *Angew. Chem., Int. Ed.* **2019,** *58*, 830-834.
45. Bruch, Q. J.; Connor, G. P.; Chen, C.-H.; Holland, P. L.; Mayer, J. M.; Hasanayn, F.; Miller, A. J. M., Dinitrogen Reduction to Ammonium at Rhenium Utilizing Light and Proton-Coupled Electron Transfer. *J. Am. Chem. Soc.* **2019,** *141*, 20198-20208.

46. Katayama, A.; Ohta, T.; Wasada-Tsutsui, Y.; Inomata, T.; Ozawa, T.; Ogura, T.; Masuda, H., Dinitrogen-Molybdenum Complex Induces Dinitrogen Cleavage by One-Electron Oxidation. *Angew. Chem., Int. Ed.* **2019,** *58*, 11279-11284.
47. Lindley, B. M.; van Alten, R. S.; Finger, M.; Schendzielorz, F.; Würtele, C.; Miller, A. J. M.; Siewert, I.; Schneider, S., Mechanism of Chemical and Electrochemical N2 Splitting by a Rhenium Pincer Complex. *J. Am. Chem. Soc.* **2018,** *140*, 7922-7935.
48. Klopsch, I.; Finger, M.; Würtele, C.; Milde, B.; Werz, D. B.; Schneider, S., Dinitrogen Splitting and Functionalization in the Coordination Sphere of Rhenium. *Journal of the American Chemical Society* **2014,** *136*, 6881-6883.
49. van Alten, R. S.; Wätjen, F.; Demeshko, S.; Miller, A. J. M.; Würtele, C.; Siewert, I.; Schneider, S., (Electro-)chemical Splitting of Dinitrogen with a Rhenium Pincer Complex. *Eur. J. Inorg, Chem.* **2020**, 1402-1410.
50. Weber, J. E.; Hasanayn, F.; Fataftah, M.; Mercado, B. Q.; Crabtree, R. H.; Holland, P. L., Electronic and Spin-State Effects on Dinitrogen Splitting to Nitrides in a Rhenium Pincer System. *Inorg. Chem.* **2021,** *60*, 6115-6124.
51. Meng, F.; Kuriyama, S.; Tanaka, H.; Egi, A.; Yoshizawa, K.; Nishibayashi, Y., Ammonia Formation Catalyzed by a Dinitrogen-Bridged Dirhenium Complex Bearing PNP-Pincer Ligands under Mild Reaction Conditions. *Angew. Chem., Int. Ed.* **2021,** *60*, 13906-13912.
52. Meng, F.; Kuriyama, S.; Egi, A.; Tanaka, H.; Yoshizawa, K.; Nishibayashi, Y., Preparation and Reactivity of Rhenium–Nitride Complexes Bearing PNP-Type Pincer Ligands toward Nitrogen Fixation. *Organometallics* **2023,** *42*, 1065-1076.
53. Cherry, J.-P. F.; Johnson, A. R.; Baraldo, L. M.; Tsai, Y.-C.; Cummins, C. C.; Kryatov, S. V.; Rybak-Akimova, E. V.; Capps, K. B.; Hoff, C. D.; Haar, C. M.; Nolan, S. P., On the Origin of Selective Nitrous Oxide N−N Bond Cleavage by Three-Coordinate Molybdenum(III) Complexes. *J. Am. Chem. Soc.* **2001,** *123*, 7271-7286.
54. Shaver, M. P.; Fryzuk, M. D., Activation of Molecular Nitrogen: Coordination, Cleavage and Functionalization of N2 Mediated By Metal Complexes. *Adv. Synth. Catal* **2003,** *345*, 1061-1076.
55. Bezdek Máté, J.; Guo, S.; Chirik Paul, J., Coordination-induced weakening of ammonia, water, and hydrazine X–H bonds in a molybdenum complex. *Science* **2016,** *354*, 730-733.
56. Matson, B. D.; Peters, J. C., Fe-Mediated HER vs N2RR: Exploring Factors That Contribute to Selectivity in P3EFe(N2) (E = B, Si, C) Catalyst Model Systems. *ACS Catal.* **2018,** *8*, 1448-1455.
57. Margulieux, G. W.; Bezdek, M. J.; Turner, Z. R.; Chirik, P. J., Ammonia Activation, H2 Evolution and Nitride Formation from a Molybdenum Complex with a Chemically and Redox Noninnocent Ligand. *J. Am. Chem. Soc.* **2017,** *139*, 6110-6113.
58. Connor, G. P.; Delony, D.; Weber, J. E.; Mercado, B. Q.; Curley, J. B.; Schneider, S.; Mayer, J. M.; Holland, P. L., Facile conversion of ammonia to a nitride in a rhenium system that cleaves dinitrogen. *Chemi. Sci.* **2022,** *13*, 4010-4018.
59. Bezdek, M. J.; Pappas, I.; Chirik, P. J., Determining and Understanding N-H Bond Strengths in Synthetic Nitrogen Fixation Cycles. In *Nitrogen Fixation*, Nishibayashi, Y., Ed. Springer International Publishing: Cham, 2017; pp 1-21.
60. Bordwell, F. G.; Cheng, J. P.; Harrelson, J. A., Homolytic bond dissociation energies in solution from equilibrium acidity and electrochemical data. *J. Am. Chem. Soc.* **1988,** *110*, 1229-1231.

61. Arashiba, K.; Eizawa, A.; Tanaka, H.; Nakajima, K.; Yoshizawa, K.; Nishibayashi, Y., Catalytic Nitrogen Fixation via Direct Cleavage of Nitrogen–Nitrogen Triple Bond of Molecular Dinitrogen under Ambient Reaction Conditions. *Bull. Chem. Soc. Jpn* **2017,** *90*, 1111-1118.
62. Klopsch, I.; Finger, M.; Würtele, C.; Milde, B.; Werz, D. B.; Schneider, S., Dinitrogen Splitting and Functionalization in the Coordination Sphere of Rhenium. *J. Am. Chem. Soc.* **2014,** *136*, 6881-6883.
63. Ostermann, N.; Rotthowe, N.; Stückl, A. C.; Siewert, I., (Electro)chemical N2 Splitting by a Molybdenum Complex with an Anionic PNP Pincer-Type Ligand. *ACS Org. Inorg. Au* **2024**.
64. Johnson, S. I.; Heins, S. P.; Klug, C. M.; Wiedner, E. S.; Bullock, R. M.; Raugei, S., Design and reactivity of pentapyridyl metal complexes for ammonia oxidation. *Chem. Commun.* **2019,** *55*, 5083-5086.
65. Nakajima, K.; Toda, H.; Sakata, K.; Nishibayashi, Y., Ruthenium-catalysed oxidative conversion of ammonia into dinitrogen. *Nature Chem.* **2019,** *11*, 702-709.
66. Schendzielorz, F. S.; Finger, M.; Volkmann, C.; Würtele, C.; Schneider, S., A Terminal Osmium(IV) Nitride: Ammonia Formation and Ambiphilic Reactivity. *Angew. Chem., Int. Ed.* **2016,** *55*, 11417-11420.
67. Pipes, D. W.; Bakir, M.; Vitols, S. E.; Hodgson, D. J.; Meyer, T. J., Reversible interconversion between a nitrido complex of osmium(VI) and an ammine complex of osmium(II). *J. Am. Chem. Soc.* **1990,** *112*, 5507-5514.
68. Askevold, B.; Nieto, J. T.; Tussupbayev, S.; Diefenbach, M.; Herdtweck, E.; Holthausen, M. C.; Schneider, S., Ammonia formation by metal–ligand cooperative hydrogenolysis of a nitrido ligand. *Nature Chemistry* **2011,** *3*, 532-537.
69. Lindley, B. M.; Bruch, Q. J.; White, P. S.; Hasanayn, F.; Miller, A. J. M., Ammonia Synthesis from a Pincer Ruthenium Nitride via Metal–Ligand Cooperative Proton-Coupled Electron Transfer. *Journal of the American Chemical Society* **2017,** *139*, 5305-5308.
70. Wang, D.; Loose, F.; Chirik, P. J.; Knowles, R. R., N–H Bond Formation in a Manganese(V) Nitride Yields Ammonia by Light-Driven Proton-Coupled Electron Transfer. *Journal of the American Chemical Society* **2019,** *141*, 4795-4799.
71. Loose, F.; Wang, D.; Tian, L.; Scholes, G. D.; Knowles, R. R.; Chirik, P. J., Evaluation of excited state bond weakening for ammonia synthesis from a manganese nitride: stepwise proton coupled electron transfer is preferred over hydrogen atom transfer. *Chemical Communications* **2019,** *55*, 5595-5598.
72. Panetti, G. B.; Kim, J.; Myong, M. S.; Bird, M. J.; Scholes, G. D.; Chirik, P. J., Photodriven Ammonia Synthesis from Manganese Nitrides: Photophysics and Mechanistic Investigations. *Journal of the American Chemical Society* **2024,** *146*, 27610-27621.
73. Lambic, N. S.; Sommer, R. D.; Ison, E. A., High-valent nitridorhenium(v) complexes containing PNP ligands: implications of ligand flexibility. *Dalton Trans.* **2018,** *47*, 758-768.
74. van der Lubbe, S. C. C.; Vermeeren, P.; Fonseca Guerra, C.; Bickelhaupt, F. M., The Nature of Nonclassical Carbonyl Ligands Explained by Kohn–Sham Molecular Orbital Theory. *Chem. Eur. J.* **2020,** *26*, 15690-15699.
75. Shanahan, J. P.; Szymczak, N. K., Hydrogen Bonding to a Dinitrogen Complex at Room Temperature: Impacts on N2 Activation. *J. Am. Chem. Soc.* **2019,** *141*, 8550-8556.
76. Evans, D. F., The determination of the paramagnetic susceptibility of substances in solution by nuclear magnetic resonance. *J. Chem. Soc.* **1959**, 2003-2005.

77. D'Alessandro, D. M.; Keene, F. R., Current trends and future challenges in the experimental, theoretical and computational analysis of intervalence charge transfer (IVCT) transitions. *Chem. Soc. Rev.* **2006,** *35*, 424-440.
78. Hush, N. S., Intervalence-Transfer Absorption. Part 2. Theoretical Considerations and Spectroscopic Data. *Prog. Inorg. Chem.* **1967,** *8*, 391-444.
79. Cundari, T. R., *Computational Organometallic Chemistry*. Taylor & Francis: 2001.
80. Chalkley, M. J.; Del Castillo, T. J.; Matson, B. D.; Peters, J. C., Fe-Mediated Nitrogen Fixation with a Metallocene Mediator: Exploring pKa Effects and Demonstrating Electrocatalysis. *J. Am. Chem. Soc.* **2018,** *140*, 6122-6129.
81. Merakeb, L.; Robert, M., Advances in molecular electrochemical activation of dinitrogen. *Curr. Opin. Electrochem.* **2021,** *29*, 100834.
82. Sherbow, T. J.; Thompson, E. J.; Arnold, A.; Sayler, R. I.; Britt, R. D.; Berben, L. A., Electrochemical Reduction of N2 to NH3 at Low Potential by a Molecular Aluminum Complex. *Eur. J. Chem.* **2019,** *25*, 454-458.
83. Pickett, C. J.; Talarmin, J., Electrosynthesis of ammonia. *Nature* **1985,** *317*, 652-653.
84. Pickett, C. J.; Ryder, K. S.; Talarmin, J., Electron-transfer reactions in nitrogen fixation. Part 2. The electrosynthesis of ammonia: identification and estimation of products. *J. Chem. Soc., Dalton Trans.* **1986**, 1453-1457.
85. Becker, J. Y.; Avraham, S., Nitrogen fixation: Part III. Electrochemical reduction of hydrazido (-NNH2) Mo and W complexes. Selective formation of NH3 under mild conditions. *J. Electroanal. Chem. Interf. Electrochem.* **1990,** *280*, 119-127.
86. Tzaguy, A.; Masip-Sánchez, A.; Avram, L.; Solé-Daura, A.; López, X.; Poblet, J. M.; Neumann, R., Electrocatalytic Reduction of Dinitrogen to Ammonia with Water as Proton and Electron Donor Catalyzed by a Combination of a Tri-ironoxotungstate and an Alkali Metal Cation. *J. Am. Chem. Soc.* **2023,** *145*, 19912-19924.
87. Bruch, Q. J.; Malakar, S.; Goldman, A. S.; Miller, A. J. M., Mechanisms of Electrochemical N2 Splitting by a Molybdenum Pincer Complex. *Inorg. Chem.* **2022,** *61*, 2307-2318.
88. Arashiba, K.; Tanaka, H.; Yoshizawa, K.; Nishibayashi, Y., Cycling between Molybdenum-Dinitrogen and -Nitride Complexes to Support the Reaction Pathway for Catalytic Formation of Ammonia from Dinitrogen. *Chem. Eur. J.* **2020,** *26*, 13383-13389.
89. Curley, J. J.; Cook, T. R.; Reece, S. Y.; Müller, P.; Cummins, C. C., Shining Light on Dinitrogen Cleavage: Structural Features, Redox Chemistry, and Photochemistry of the Key Intermediate Bridging Dinitrogen Complex. *J. Am. Chem. Soc.* **2008,** *130*, 9394-9405.
90. Tanabe, Y.; Sekiguchi, Y.; Tanaka, H.; Konomi, A.; Yoshizawa, K.; Kuriyama, S.; Nishibayashi, Y., Preparation and reactivity of molybdenum complexes bearing pyrrole-based PNP-type pincer ligand. *Chem. Commun.* **2020,** *56*, 6933-6936.
91. Magnuson, R. H.; Taube, H., Mixed oxidation states in osmium ammine dinitrogen complexes. *J. Am. Chem. Soc.* **1972,** *94*, 7213-7214.
92. Lay, P. A.; Magnuson, R. H.; Taube, H.; Sen, J., Synthesis of (trifluoromethanesulfonato)pentaammineosmium(III): osmium(III) pentaammine complexes. *J. Am. Chem. Soc.* **1982,** *104*, 7658-7659.
93. Richardson, D. E.; Sen, J. P.; Buhr, J. D.; Taube, H., Preparation and properties of mixed-valence (.mu.-dinitrogen)bis(pentaammine) complexes of osmium and ruthenium. *Inorg. Chem.* **1982,** *21*, 3136-3140.

94. Kunkely, H.; Vogler, A., Photolysis of Aqueous [(NH3)5Os(μ-N2)Os(NH3)5]5+: Cleavage of Dinitrogen by an Intramolecular Photoredox Reaction. *Angew. Chem., Int. Ed.* **2010,** *49*, 1591-1593.
95. Krewald, V.; González, L., A Valence-Delocalised Osmium Dimer capable of Dinitrogen Photocleavage: Ab Initio Insights into Its Electronic Structure. *Chem. Eur. J.* **2018,** *24*, 5112-5123.
96. Tanabe, Y.; Nishibayashi, Y., Comprehensive insights into synthetic nitrogen fixation assisted by molecular catalysts under ambient or mild conditions. *Chem. Soc. Rev.* **2021,** *50*, 5201-5242.
97. van Alten, R. S.; Wieser, P. A.; Finger, M.; Abbenseth, J.; Demeshko, S.; Würtele, C.; Siewert, I.; Schneider, S., Halide Effects in Reductive Splitting of Dinitrogen with Rhenium Pincer Complexes. *Inorg. Chem.* **2022,** *61*, 11581-11591.
98. Dhar, D.; Yee, G. M.; Spaeth, A. D.; Boyce, D. W.; Zhang, H.; Dereli, B.; Cramer, C. J.; Tolman, W. B., Perturbing the Copper(III)–Hydroxide Unit through Ligand Structural Variation. *Journal of the American Chemical Society* **2016,** *138*, 356-368.
99. Pratt, D. A.; DiLabio, G. A.; Mulder, P.; Ingold, K. U., Bond Strengths of Toluenes, Anilines, and Phenols: To Hammett or Not. *Accounts of Chemical Research* **2004,** *37*, 334-340.
100. Serrano, I.; Sala, X.; Plantalech, E.; Rodríguez, M.; Romero, I.; Jansat, S.; Gómez, M.; Parella, T.; Stoeckli-Evans, H.; Solans, X.; Font-Bardia, M.; Vidjayacoumar, B.; Llobet, A., Synthesis, Structure, Redox Properties, and Catalytic Activity of New Ruthenium Complexes Containing Neutral or Anionic and Facial or Meridional Ligands: An Evaluation of Electronic and Geometrical Effects. *Inorganic Chemistry* **2007,** *46*, 5381-5389.
101. Stuyver, T.; De Proft, F.; Geerlings, P.; Shaik, S., How Do Local Reactivity Descriptors Shape the Potential Energy Surface Associated with Chemical Reactions? The Valence Bond Delocalization Perspective. *J. Am. Chem. Soc.* **2020,** *142*, 10102-10113.
102. Gau, M. R.; Keller, T. M.; Scepaniak, J. J., An Atypically Bent Isocyanide at Iron In A Tetrapodal Penta-Carbene Framework. *Eur. J. Inorg, Chem.* **2024,** *27*, e202400146.
103. Jones, W. D.; Foster, G. P.; Putinas, J. M., Preparation and structural examination of a series of new, low-valent iron phosphine isocyanide complexes with bent carbon-nitrogen-carbon linkages. *Inorg. Chem.* **1987,** *26*, 2120-2127.
104. Kiernicki, J. J.; Zeller, M.; Szymczak, N. K., Requirements for Late-Stage Hydroboration of Pyridine N-Heterocyclic Carbene Iron(0) Complexes: The Role of Ancillary Ligands. *Organometallics* **2021,** *40*, 2658-2665.